Applied Catalysis A, General 647 (2022) 118900

Contents lists available at ScienceDirect

Applied Catalysis A, General

journal homepage: www.elsevier.com/locate/apcata

The role of promoters on the catalytic performance of $M_xV_2O_5$ bronzes for the selective partial oxidation of H_2S

Lidia Ruiz-Rodríguez [a], Agustín de Arriba [a], Alejandro Vidal-Moya [a], Teresa Blasco [a], Enrique Rodríguez-Castellón [b], José M. López Nieto [a,*]

[a] Instituto de Tecnología Química, Universitat Politècnica de València-Consejo Superior de Investigaciones Científicas, Avenida de los Naranjos s/n, 46022 Valencia, Spain

[b] Departamento de Química Inorgánica, Facultad de Ciencias, Universidad de Málaga, 29071 Málaga, Spain

ARTICLE INFO

Keywords:
Vanadium oxide bronze
Catalysts
Partial oxidation of hydrogen sulfide
Sulfur formation

ABSTRACT

Metal-containing vanadium oxide bronzes ($M_xV_2O_5$; M= Cu, Ag and Ca) have been prepared, characterized (before and after reaction) by various physicochemical techniques, and tested in the partial oxidation of H_2S. The catalysts were prepared hydrothermally at 175 °C (from gels containing M/V molar ratios of 0.17 or 0.33) and heat-treated at 500 °C/2 h in N_2. The most effective catalysts, showing a sulfur selectivity greater than 95 % for a H_2S conversion beyond 90 %, were those presenting vanadium oxide bronze (β-$Cu_{0.261}V_2O_5$ or $Ag_{0.333}V_2O_5$) as the main crystalline phase. Cu- and Ag-containing vanadium oxide bronzes were stable under reaction conditions. For calcium containing materials (mainly presenting the $Ca_{0.17}V_2O_5$ bronze phase), the formation of $CaSO_4$ has been observed during the reaction, which resulted in a negative effect on both activity and selectivity. The nature of active and selective sites in this type of catalysts, as well as the role of promoters, are also discussed.

1. Introduction

Hydrogen sulfide (H_2S) is a well-known by-product in a wide range of petrochemical processes, and due to its critical environmental impact (responsible, for instance, of the acidic rain), its uncontrolled emission to the atmosphere must be stopped. Nowadays, most of the H_2S emissions in petrochemical industries are attenuated by the Claus Process, but its efficiency is nearly exhausted. Therefore, most efforts are now directed towards developing additional processes of interest to treat both the crude oil and the natural gas. In this sense, cleaning processes of the tail gases have caught lots of attention [1–4].

Among all the different alternatives, an interesting approach is the partial oxidation of H_2S to elemental sulfur under gaseous conditions [1,2], being the catalysts based on unsupported and supported V_2O_5 (orthorhombic structure, *D2h*) [5–18] the ones with the best performance. However, it has been shown that, under the reaction conditions used for H_2S partial oxidation (temperatures lower than 220 °C), V_2O_5 is selectively transformed into V_4O_9 (orthorhombic, *Cmcm*), a partially reduced vanadium oxide [8,14]. It is suggested that the presence of V^{4+}-O-V^{5+} pairs in the V_4O_9 is the responsible for the high selectivity to elemental sulfur, by diminishing further over-oxidation to SO_2 [8], which is known to be a pollutant as well as H_2S.

On the other hand, for supported vanadium oxide catalysts, it has been proposed that the strong interaction between the active V-atoms, not fully oxidized, and the support (TiO_2), favors the formation of oxygen vacancies and, consequently, a rapid catalyst regeneration (re-oxidation of V^{4+} to V^{5+}) is facilitated [12,13,15]. Thus, it can be expected that the environment, the coordination and the oxidation state of V-atoms have a strong influence on both the activity for hydrogen sulfide oxidation and the selectivity to sulfur.

Furthermore, it has been proposed that during the reaction over oxides derived from Mg/Al-$V_{10}O_{28}$ layered double hydroxides, the gradually produced sulfate anions could react with V^{4+} species to form less active $VOSO_4$, which could favor the re-oxidation of V-species, improving the redox properties of V^{5+} [17].

Moreover, selectivity to sulfur during the partial oxidation of H_2S over vanadium oxide can also be improved by doping the vanadium oxide catalysts with alkali metals, especially Na^+ cations, which favor the transformation of V_2O_5 into metal-doped vanadium oxide bronze [19]. Thus, Na-containing catalysts, forming the NaV_6O_{15} bronze phase [20], were reported to be active and very selective for the oxidation of H_2S to sulfur. According to recent studies on metal-containing vanadium

* Corresponding author.
E-mail address: jmlopez@itq.upv.es (J.M. López Nieto).

https://doi.org/10.1016/j.apcata.2022.118900
Received 2 August 2022; Received in revised form 20 September 2022; Accepted 6 October 2022
Available online 11 October 2022

oxide bronzes, the catalytic properties change depending on the acid-basic and/or redox characteristics of the metal dopant. Nevertheless, the hydrothermal synthesis of these metal-containing vanadium bronzes strongly depends on the metal precursors and the *M*/V ratio [21,22]. However, the catalytic performance of metal-doped vanadium oxide bronze could be modified by incorporating atoms with redox properties (such as Ag or Cu) or divalent cations (such as Ca).

This work comparatively studies the synthesis of Ag-, Cu- and Ca-promoted vanadium oxides presenting the crystalline phase β-$M_xV_2O_5$, using different amounts of promoter (and metal carboxylate as precursor). Thus, *M*-containing V_2O_5 materials (*M*= Ag, Cu and Ca) were prepared hydrothermally (from aqueous gels containing V_2O_5/H_2O_2/*M*X mixtures), with *M*/V ratios of 0.17 and 0.33. Finally, these materials have been tested as catalysts for the partial oxidation of H_2S to elemental sulfur. In addition, used catalysts were also studied to ascertain both their structural stability and their different catalytic properties.

2. Experimental

2.1. Preparation of catalysts

The vanadium oxide bronze-type catalysts have been hydrothermally synthesized from an aqueous solution of V_2O_5, H_2O_2 and the appropriate amount of the metal precursor (i.e. *M*/V atomic ratio of 0.17 or 0.33; M= Ag, Cu, Ca): silver(I) acetate ($AgC_2H_3O_2$), copper(I) acetate ($CuC_2H_3O_2$) and calcium oxalate (CaC_2O_4), from Sigma-Aldrich. The aqueous gels were subsequently autoclaved at 175 °C for 72 h and thermally activated at 500 °C for 2 h under a N_2 stream. The catalysts have been named as ***M*/V-x** (*M*= Ag, Cu or Ca), in which x is the *M*/V molar ratio in the synthesis gel; i.e. 0.17 or 0.33. In addition to these, bulk V_2O_5 has been prepared by calcination at 500 °C of ammonium metavanadate precursor for comparative purposes. This sample has been named as **V_2O_5**. On the other hand, V_4O_9 was prepared by heat-treatment of **V_2O_5** sample at 200 °C, for 2 h, in a mixture of H_2S/Air/He with a molar ratio of 1.2/5.0/83.8 (total flow 20 mL min^{-1} per gram of catalyst) [14].

2.2. Characterization of catalysts

X-ray diffraction (XRD) patterns of powder solids were collected with a PANalytical CUBIX instrument equipped with a graphite monochromator, employing Cu Kα radiation (λ = 0.1542 mm) and operating at 45 kV and 4 mA. The distribution of the crystalline phases in the catalysts was calculated by Rietveld refinement of the XRD patterns employing XPert Highscore Plus software.

IR spectra were measured in the 300–3900 cm^{-1} region with a Nicolet 710 FTIR spectrometer, with a spectral resolution of 1 cm^{-1} and 128 accumulations per scan.

The specific surface areas have been determined by the BET method from N_2 adsorption isotherms at − 196 °C measured in a Micromeritics TriStar 3000 instrument.

Raman spectra were recorded with an "in via" Renishaw spectrometer equipped with an Olympus microscope. The samples were generally excited by the 514.5 nm line of an Ar^+ laser (Spectra Physics model 171) with a laser power of 2.5 mW [18].

Temperature-programmed reduction experiments (H_2-TPR) were performed in a Micromeritics Autochem 2910 equipped with a TCD detector. The reducing gas composition was 10 % H_2 in Ar, with a total flow rate of 50 mL min^{-1}. The materials were heated until 800 °C, at a heating rate of 10 °C min^{-1}.

X-ray photoelectron spectroscopy (XPS) measurements were performed on a SPECS spectrometer equipped with a Phoibos 150 MCD-9 detector using a monochromatic Al Kα (1486.6 eV) X-ray source. Spectra were recorded using an analyzer pass energy of 50 eV, an X-ray power of 100 W, and an operating pressure of 10^{-9} mbar. Spectra treatment was performed using CASA software. Binding energies (BE) were referenced to C *1s* at 284.5 eV.

EPR spectra were obtained at − 170 °C using an EMX-12 Bruker spectrometer working at the X band, with a frequency modulation of 100 kHz and 1 G amplitude.

Quantitative EDX analysis were carried out using an Oxford LINK ISIS System with the SEMQUANT program coupled to a JEOL 6300 microscope operating at 20 kV, where scanning electron microscopy (SEM) images were collected.

2.3. Catalytic tests

Catalytic experiments for the H_2S partial oxidation to elemental sulfur were carried out in a quartz tubular fixed-bed reactor at atmospheric pressure and a reaction temperature of 180 °C up to 300 min. Catalyst loading (0.1 g) was diluted with silicon carbide in order to achieve the optimal bed height to avoid homogeneous reactions. The feed consisted of a mixture of H_2S/Air/He with a molar ratio of 1.2/5.0/83.8, and a total flow of 130 mL min^{-1} (contact time, W/F, of 31.2 g_{cat} h mol^{-1}_{H2S}). The analysis of the reaction products, as well as the reactants, was performed by online gas chromatography using two different chromatographic columns [8]: i) Molecular Sieve 5 Å for N_2 and O_2 separation; and ii) Porapak T for H_2S and SO_2 analysis. In addition to this, a condenser was located at the bottom of the reactor to trap the sulfur gas content in the effluent stream. In this sense, both the conversion of H_2S and the sulfur selectivity were defined as follows:

1) H_2S conversion (%) = (moles of H_2S reacted/moles of H_2S fed) x 100
2) S selectivity = (moles of H_2S reacted – moles of SO_2 produced)/(moles of H_2S reacted) x 100

3. Results and discussion

3.1. Characterization of catalysts

The main characteristics of the catalysts heat-treated at 500 °C in an inert atmosphere are shown in Table 1. The Ca-containing samples possess surface areas of ca. 16 m^2 g^{-1}, while those containing Cu or Ag show similar values of ca. 8 m^2 g^{-1}.

Fig. 1 shows the XRD patterns of the *M*-containing catalysts with *M*/V atomic ratio of 0.17 and 0.33, in addition to pure vanadium oxide catalyst (i.e. V_2O_5) and the corresponding partially reduced one (i.e. V_4O_9) which were also included for comparison.

For the metal-promoted catalysts (*M*= Ag, Cu and Ca), the corresponding vanadium-bronze phase is the predominant crystalline structure: $Ag_{0.333}V_2O_5$ [JCPDS: 1–81–1740], $Cu_{0.261}V_2O_5$ [JCPDS: 1–79–0796] and $Ca_{0.17}V_2O_5$ [JCPDS: 26–1165]. However, minor amount of other crystalline phases such as orthorhombic α-V_2O_5 [JCPDS: 41–1426], $Ag_{1.2}V_3O_8$ [JCPDS: 88–0686] or CuV_2O_6 [JCPDS: 1–74–2117] are also observed depending on the *M*/V atomic ratio in the synthesis gel (Table 1).

Noteworthy, the catalysts promoted with Ca (i.e. samples **Ca/V-0.17** and **Ca/V-0.33**) uniquely present the β-MV_2O_5 phase, β-$Ca_{0.17}V_2O_5$.

The infrared spectra in the 1100–500 cm^{-1} region of *M*-containing catalysts are shown in Fig. 2a–c, whereas the corresponding spectra of the undoped vanadium oxide samples (i.e. V_2O_5 and V_4O_9) are shown in Fig. 2d. In addition, the corresponding IR spectra in the 1050–850 cm^{-1} region are presented in Fig. S1.

The IR spectrum of undoped vanadium oxide, **V_2O_5**, shows intense bands at 1020, 830 and 610 cm^{-1}, assigned to V=O stretch, V-O-V stretching modes and bending vibrations [23,24], respectively, (Fig. 2d and Fig. S1). However, V_4O_9 shows bands (or shoulders) at 977, 950, 921, 905, 842 , 723 and 540 cm^{-1} (Fig. 2d and Fig. S1), in agreement to previous results [25,26].

The main bands of V_2O_5 disappear or shift to lower values in doped-vanadium oxide bronzes (Fig. 2 and Figs. S2–S4). Thus, the band at 1020 cm^{-1} appears as a small band in the 1000–950 cm^{-1} range depending on both metal and metal-loading, which can be related to a

Table 1
Characteristics of catalysts heat-treated at 500 °C in inert atmosphere.

Sample	*M*/V	S_{BET}	Crystalline phases (XRD)[b]		TPR results[c]	
	Atomic ratio[a]	(m^2 g^{-1})	Majority	Minority	TCM (°C)	H_2-uptake
V_2O_5	0	5.9	V_2O_5	–	637 (689, 729)	12.8
Ag/V-0.17	0.16	8.1	β-$Ag_{0.333}V_2O_5$	–	420 (481)	11.8
Cu/V-0.17	0.11	7.1	β-$Cu_{0.261}V_2O_5$	V_2O_5	474 (516)	13.4
Ca/V-0.17	0.15	13.4	β-$Ca_{0.17}V_2O_5$	–	621 (697)	9.4
Ag/V-0.33	0.33	n.d.	β-$Ag_{0.333}V_2O_5$	$Ag_{1.2}V_3O_8$	367 (461)	11.0
Cu/V-0.33	0.28	8.8	β-$Cu_{0.261}V_2O_5$	CuV_2O_6	417	13.2
Ca/V-0.33	0.30	16.7	β-$Ca_{0.17}V_2O_5$	–	621 (715)	6.7

a) M/V ratio calculated by EDX on heat-treated solids.
b) Crystalline phases detected by XRD in fresh catalysts.
c) TPR-H_2 results: Temperature of the first maximum hydrogen consumption (TCM), in parenthesis other reduction peaks; and H_2-uptake (in $mmol_{H2}$ g_{cat}).

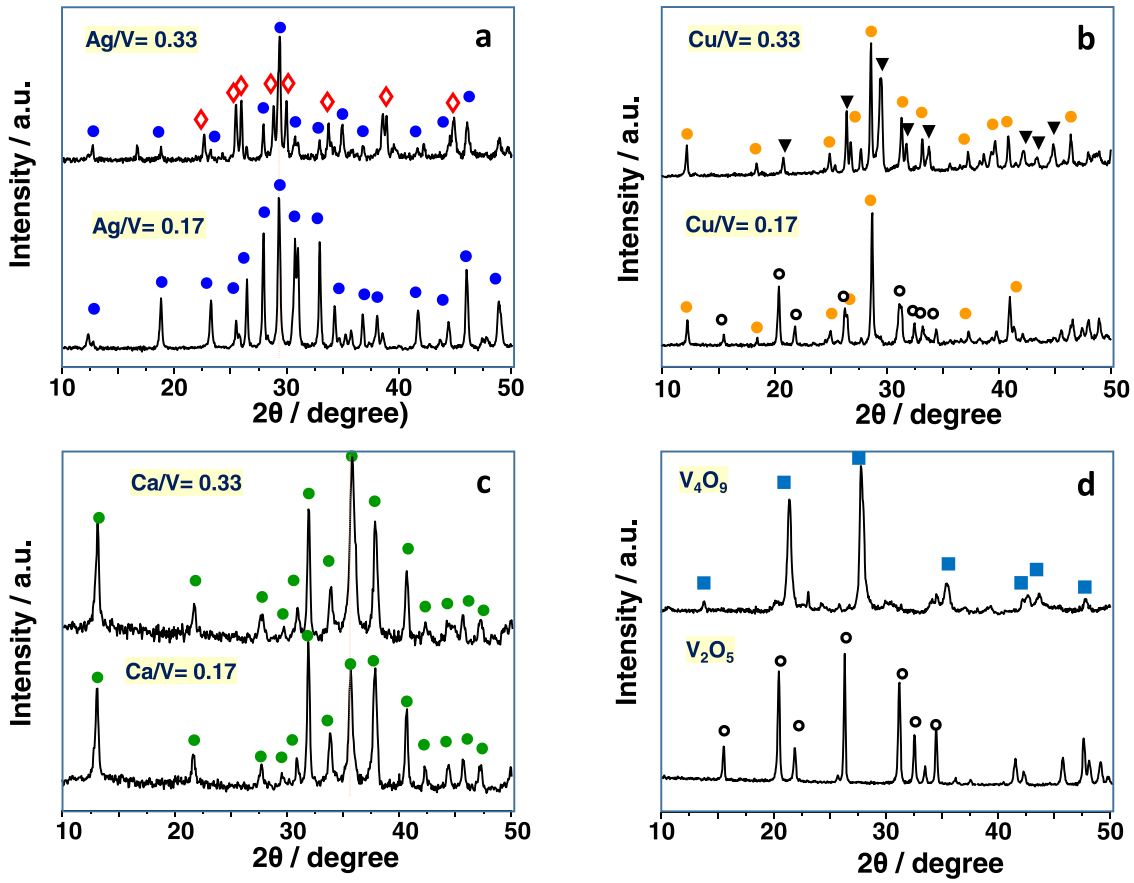

Fig. 1. XRD patterns of heat-treated M-containing vanadium oxide bronzes, with *M*/V ratios of 0.17 or 0.33; and *M*= Ag^+ (a), Cu^+ (b), or Ca^{2+} (c), as promoters. For comparison it has been also included the XRD pattern of unpromoted vanadium oxides (d), i.e. V_2O_5 and V_4O_9. Symbols corresponds to pure phases: (●) β-$Ag_{0.33}V_2O_5$ (JCPDS: 0–81–1740); (◊) $Ag_{1.2}V_3O_8$ (JCPDS: 0–88–0686); (●) β´-$Cu_{0.261}V_2O_5$ (JCPDS: 1–79–0796); (▼) CuV_2O_6 (JCPDS: 1–74–2117); (●) β-$Ca_{0.17}V_2O_5$ (JCPDS: 0–26–1165); (○) V_2O_5 (JCPDS: 0–09–0387); (■) V_4O_9 (JCPDS: 0–23–0720).

decrease of the binding strength and of the stretch vibration of the V=O bond by the incorporation of the different metals [23–27]. In addition, bands located at 830 and 610 cm^{-1} in V_2O_5 have not been observed for *M*-containing vanadium oxide bronzes, although other new bands appeared.

In Ag-containing samples (Figs. 2a, and S2), it is observed the presence of intense bands at 984 and 970 cm^{-1}, whose relative intensities change with the Ag-content. Less intense bands at 1005, 954, 935 and 920 cm^{-1}, detected in the spectrum of sample **Ag/V-0.17**, can be related to the presence of $Ag_{0.33}V_2O_5$ [28]. However, in the case of the **Ag/V-0.33** sample, in addition to the bands related to $Ag_{0.33}V_2O_5$, new bands are observed at 970, 917 and 879 cm^{-1} which are ascribed to the presence of $Ag_{1.2}V_3O_8$, in agreement to XRD patterns (Fig. 1a).

In the case of Cu-containing samples (Figs. 2b, and S3), clear changes are observed depending on the Cu-loading. Thus, the IR spectrum of sample **Cu/V-0.17** exhibits a narrow band at 1010 cm^{-1}, a shoulder at 975 cm^{-1}, and a band at 820 cm^{-1}, which are attributed to the stretching vibration of multiple V=O bonds [29]. On the contrary, the intensity of these bands is significantly attenuated in the spectrum of the **Cu/V-0.33** catalyst, as reported previously for $Cu_xV_2O_5$ nanowires [29]. In addition to this, the spectrum clearly shows the characteristic bands of the bronze β´-$Cu_{0.261}V_2O_5$ (in the region between 950 and 800 cm^{-1}), assigned to the V-O-V and V-O stretching vibrations in interaction with Cu^+/Cu^{2+}. Moreover, the displacement of the bands, with a broad band centered at 1010 cm^{-1}, and additional bands at 888, 850, 613 and 563 cm^{-1}, caused by the presence of both V^{5+} and V^{4+} species is also

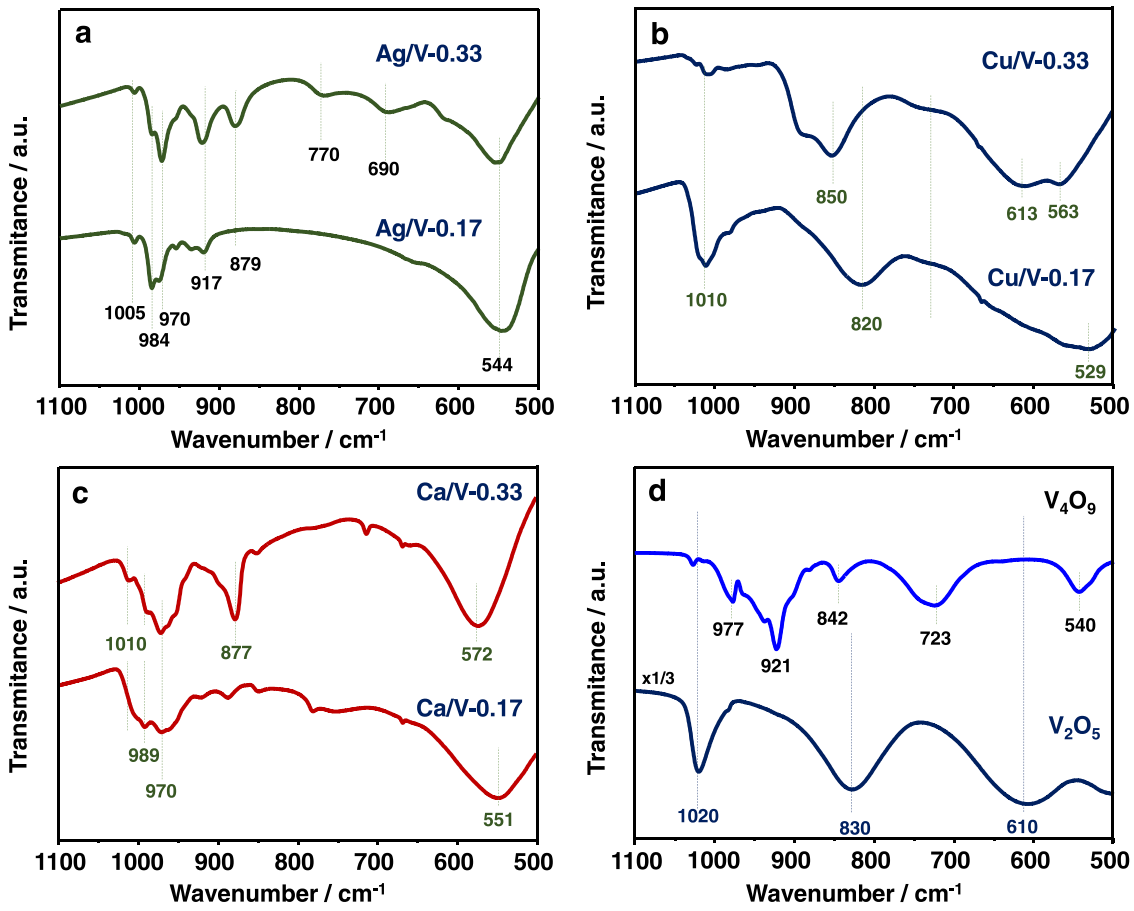

Fig. 2. FTIR spectra of heat-treated samples: a) **Ag/V-0.17** and **Ag/V-0.33**; b) **Cu/V-0.17** and **Cu/V-0.33**; c) **Ca/V-0.17** and **Ca/V-0.33**; d) $\mathbf{V_2O_5}$ and V_4O_9.

reported [30].

Lastly, for Ca-containing samples, the characteristic bands of monoclinic bronze β-$Ca_{0.17}V_2O_5$ are observed at 994 and 970 cm^{-1} (related to V=O bonds, in vanadium atoms with different oxidation states) and ca. 551 cm^{-1} (assigned to the V-O-V and VO···Ca^{2+} links). In addition, the catalyst **Ca/V-0.33** presents characteristic peaks of the $CaCO_3$ crystalline phase, with bands at 877 cm^{-1} (vibration of the CO_3^{2-} group) and 713 cm^{-1} (assigned to the Ca-O bond) [31].

Thus, the new bands appearing in the 1010–975 cm^{-1} range in the spectra of *M*-doped catalysts, correspond to the $\nu(V^{5+}=O)$ and $\nu(V^{4+}=O)$ stretching modes, but also suggests an effective incorporation of Ag^+, Cu^+ and Ca^{2+} cations in the vanadium bronze structure and the formation of the selective V^{5+}-O-V^{4+} pairs [27,28].

The H_2-TPR results for the catalysts heat-treated at 500 °C/N_2 are shown in Fig. 3, while their H_2 consumption is presented in Table 1. For comparison, it has been also included the reduction pattern of V_2O_5, characterized by the presence of three peaks at 637, 669 and 729 °C [19,23]. In addition, the reduction maxima of the catalysts doped with Ag and Cu shift to lower temperatures indicating that they present a higher reducibility than the $\mathbf{V_2O_5}$ catalyst. Meanwhile, the reducibility of Ca-containing catalysts (i.e. **Ca/V-0.17** and **Ca/V-0.33** samples) is similar to that of undoped vanadium oxide ($\mathbf{V_2O_5}$), with a reduction maximum at around 621 °C, being the first peak more intense than that observed for V_2O_5 ($\mathbf{V_2O_5}$). In any case, for every series, a higher reducibility is observed for the ***M*/V-0.33** catalysts compared to their ***M*/V-0.17** counterpart.

With respect to the H_2-consumption during the TPR experiments (Table 1), a slight decrease is observed for the promoted catalysts. However, it is not possible to calculate the amount related to V-species, since both copper and silver could also be reduced under these experimental conditions. Nevertheless, the temperature of reduction of the catalysts increases according to the following trend: **Ag/V-0.33** < **Ag/V-0.17** ≈ **Cu/V-0.33** < **Cu/V-0.17** < **Ca/V-0.33** ≈ **Ca/V-0.17** ≈ $\mathbf{V_2O_5}$.

The chemical composition on the surface of the catalysts doped with the three metals was studied by XPS. Fig. 4 plots the XPS spectra of the V $2p_{3/2}$ core level of the ***M*/V-0.17** (Fig. 4A) and the ***M*/V-0.33** (Fig. 4B) series. All spectra show two contributions at binding energies of 517.5 and 516.1 eV, corresponding to V^{5+} and V^{4+} species, respectively [32]. In Table 2 it can be seen the V^{4+}/V^{5+} ratio for ***M*/V-0.17** and ***M*/V-0.33** catalysts heat-treated at 500 °C in inert atmosphere.

In addition to this, the Ag *3d*, Cu $2p_{3/2}$ and Ca *2p* and core level spectra, shown in Fig. S5, indicate the unique presence of Ag^+ and Ca^{2+} species in catalysts with Ag/V and Ca/V ratios of 0.17 or 0.33. Meanwhile, the analysis of the spectra of both **Cu/V-0.17** and **Cu/V-0.33** catalysts, allows us to identify signals at 932.2 and 934.3 eV, as well as the characteristic shake-up satellites, indicating the presence of a mixture of Cu^+/Cu^{2+} species [33].

Fig. 5 shows the EPR spectra of the ***M*/V-0.17** and ***M*/V-0.33** series and the different components used for their simulation, whereas Table 2 summarizes EPR results of the catalysts. For comparison, the spectrum of V_4O_9 has been also included (Fig. S6).

The signals of paramagnetic V^{4+} ($3d^1$) species contained in all catalysts are isotropic and of Lorentzian shape with varying widths, indicating that there is an interaction between neighboring V^{4+} sites connected through the oxygen bridges. This is supported by the absence of non-symmetric signal associated to isolated VO^{2+} species with a hyperfine structure due to the interaction of the unpaired electron with the vanadium nuclei (I=7/2) [34]. Interestingly, the spectra of the Cu-containing samples contain, besides the signal of vanadium, another

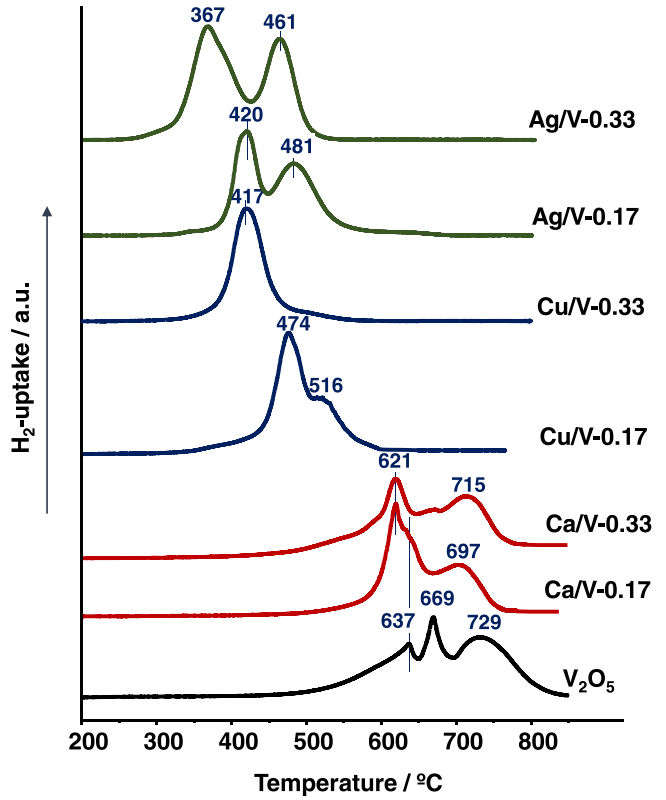

Fig. 3. H_2-TPR patterns of ***M*V-0.17** and ***M*V-0.33** catalysts (*M*= Ca, Cu or Ag). For comparison it has been also included the TPR pattern of an undoped vanadium oxide (**V_2O_5** sample).

axially symmetric signal due to $Cu^{2+}(d^9)$ with a hyperfine structure coming from the interaction of the unpaired electron with the nuclear spin of the copper (I = 3/2) ($g_{//} = 2.31$ $A_{//} = 117$ G, $g_{\perp} = 2.05$) (Fig. S7) [36]. This gives rise to a quadruplet which is well resolved in the parallel region of the signal and not in the perpendicular one.

The spectra of all samples consist mostly of a broad signal of V^{4+} with a width in the range 200–300 G, except those of the **Ca/V-0.17** and **Ag/V-0.33** samples. The spectrum of the **Ca/V-0.17** catalyst is formed by two components of 120 G and 38 G wide accounting for 30% and 70% of total intensity, respectively. However, the EPR spectrum of the **Ag/V-0.33** catalyst displays two superimposed very narrow (60 G and 28 G) signals of equal intensity. Broad EPR signals are indicative of weak spin-spin exchange among V^{4+} usually associated to small clusters, while stronger spin exchange produces narrower signals. Therefore, paramagnetic vanadium species are more coupled in the **Ca/V-0.17** sample, and especially in the **Ag/V-0.33** catalyst, suggesting that they are closer to a bulk-structure with more vanadyl sites in close proximity.

3.2. *Catalytic tests for partial oxidation of hydrogen sulfide*

Fig. 6 compares the variation of H_2S conversion with time at 180 °C for both ***M*/V-0.17** and ***M*/V-0.33** series of catalysts. In all cases, elemental sulfur and sulfur oxide (as minority) were mainly observed, in agreement to previous results reported for vanadium based catalysts [5–18]. In addition, the variation of the selectivity to SO_2 with time on stream is presented in Fig. S8. Accordingly, a selectivity to sulfur higher than 80% is observed in all cases. In general, the selectivity to SO_2 decreases initially with time on stream, suggesting the elimination of less selective oxygen species on the catalyst surface.

The catalytic results show that the H_2S conversion initially decreases with time on stream, which could be related to a stabilization of the catalyst under reaction conditions. The **Cu/V-0.17**, **Cu/V-0.33** and **Ag/V-0.17** catalysts seem to be the most stable, with H_2S conversions up to

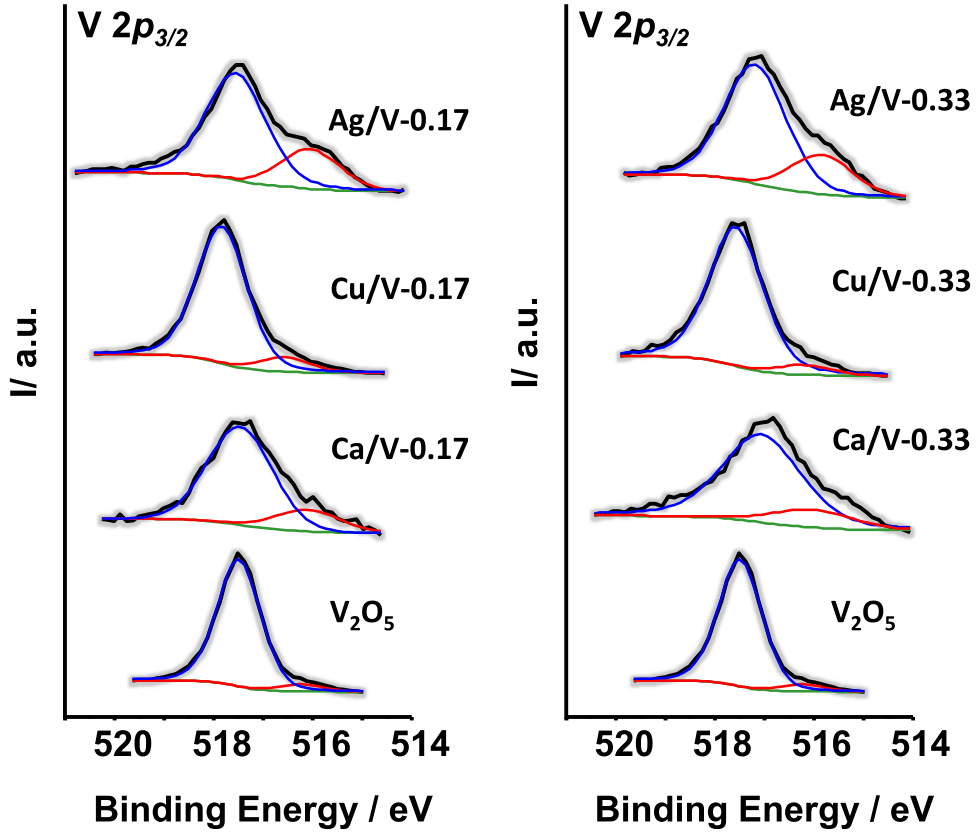

Fig. 4. XPS V $2p_{3/2}$ core level spectra of the ***M*/V-0.17** (A) and ***M*/V-0.33** (B) series. Samples were heat-treated at 500 °C in N_2.

Table 2
XPS and EPR characterization of catalysts.

Sample	XPS (fresh samples)[a]		XPS (used samples)[b]		EPR components[a, c]		
	M/V ratio	V^{4+}/V^{5+} ratio	V^{4+}/V^{5+} ratio	$S^{2-}/S^0/SO_4^{2-}$ ratio	ΔH_{PP}/G (I/%)	ΔH_{PP}/G (I/%)	wt% V^{4+}
V_2O_5	0	8/92	29/71	0/66/34			
Ag/V-0.17	0.20	25/75	33/67	0/12/88	240	–	3.1
Cu/V-0.17	0.20	13/87	44/56	45/38/17	277		0.43
Ca/V-0.17	0.23	16/84	23/77	0/20/80	110 (30%)	38 (60%)	1.49
Ag/V-0.33	0.44	24/76	27/73	30/0/70	60 (50%)	24.5 (50%)	0.92
Cu/V-0.33	0.47	11/89	29/71	37/26/37	295		1.41
Ca/V-0.33	0.39	18/82	13/87	0/34/67	197 (95%)	89.0 (5%)	1.82

a) Samples heat-treated at 500 °C for 2 h in N_2.
b) Catalysts after catalytic tests.
c) The width of the signal is given in G and its relative intensity within the parenthesis. The signal of Cu^{2+} accounts for 0.2 % and 2.0 % of the total intensity of the spectra for the **Ag/V-0.33** and **Ag/V-0.17**, respectively.

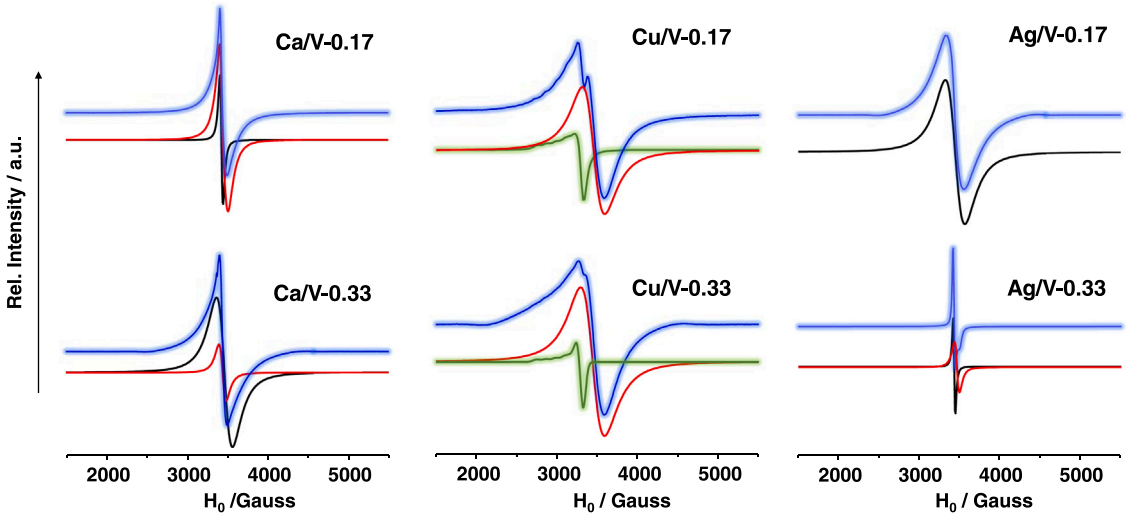

Fig. 5. EPR spectra (blue line) of ***M*V-0.17** and ***M*V-0.33** catalysts (*M*= Ca, Cu or Ag), heat-treated in N_2 at 500 °C, and the components used for their simulation. The green components in the spectra of the Cu/V catalysts correspond to the contribution of paramagnetic Cu^{2+}.

90% for **Cu/V-0.17** and about 97% for both **Cu/V-0.33** and **Ag/V-0.17** at reaction times up to 4 h.

On the other hand, the **Ag/V-0.33** catalyst shows important changes with the reaction time (with a H_2S conversion of ca. 20 % after 5 h), suggesting some modifications of the catalyst under the reaction conditions (see latter discussion).

Moreover, the H_2S conversion is similar for both **Ca/V-0.17** and **Ca/V-0.33,** slightly decreasing with the reaction time (below 80 % at 5 h), while the **V_2O_5** catalyst reaches a H_2S conversion of around 60 % after 4 h of reaction time, in good agreement with previous results. The *M*/V ratio has a very low influence on the H_2S conversion for Ca-containing catalysts, and very high influence for Ag-containing catalysts.

The variation of the elemental sulfur selectivity with the H_2S conversion for these catalysts is presented in Fig. 7. Metal promoted catalysts with *M*/V ratio in the synthesis gel of 0.17 are more selective to elemental sulfur than the undoped **V_2O_5** sample, even at H_2S conversion values above 90 %. On the contrary, for the catalysts with the highest metal-loading, the selectivity to sulfur in the case of **Ag/V-0.33** (Fig. 7A) **Ca/V-0.33** (Fig. 7C) catalysts is lower than that of **V_2O_5**, whereas the **Cu/V-0.33** catalyst shows higher selectivity than the undoped vanadium oxide catalyst (Fig. 7B).

In conclusion, the selectivity to sulfur is lower in the ***M*/V-0.33** series than their ***M*/V-0.17** series counterpart, even for the catalyst containing copper (Cu/V-0.33), especially notorious at H_2S conversions beyond 90%. In any case, these results suggest that the incorporation of Cu into

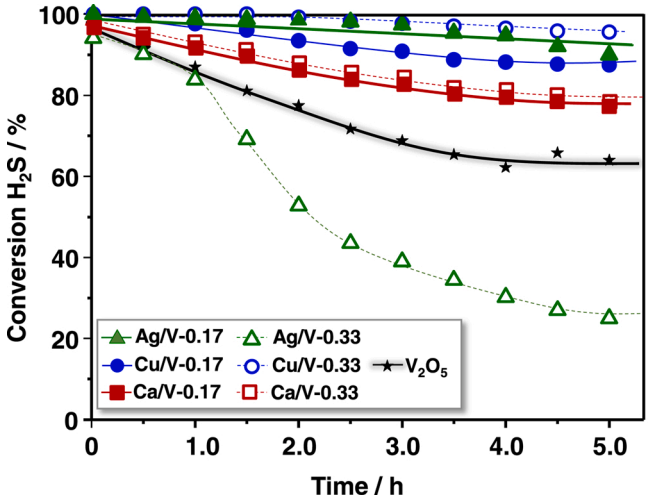

Fig. 6. Variation of the H_2S conversion with time on stream for both **M/V-0.17** and **M/V-0.33** series, M= Ag; Cu or Ca. For comparison, the catalytic results of undoped vanadium oxide (**V_2O_5**) have been also included. Reaction conditions: T = 180ºC; H_2S/Air/He molar ratio of 1.2/5.0/83.8; contact time, W/F, of 31.2 g_{cat} h mol^{-1}_{H2S}.

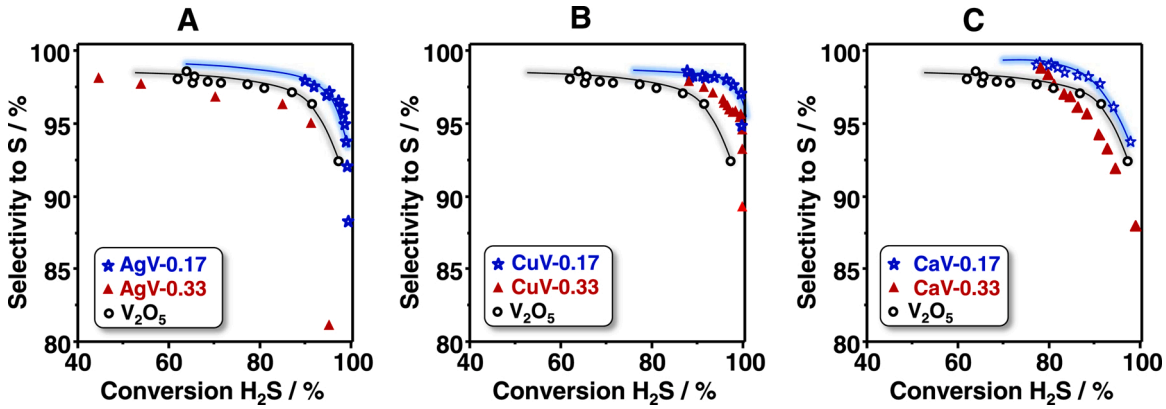

Fig. 7. Variation of the elemental sulfur selectivity during the partial oxidation of H_2S over: A) **Ag/V-0.17** and **Ag/V-0.33**, B) **Ca/V-0.17** and **Ca/V-0.33** and C) **Cu/V-0.17** and **Cu/V-0.33** catalysts. Reaction conditions as in Fig. 6.

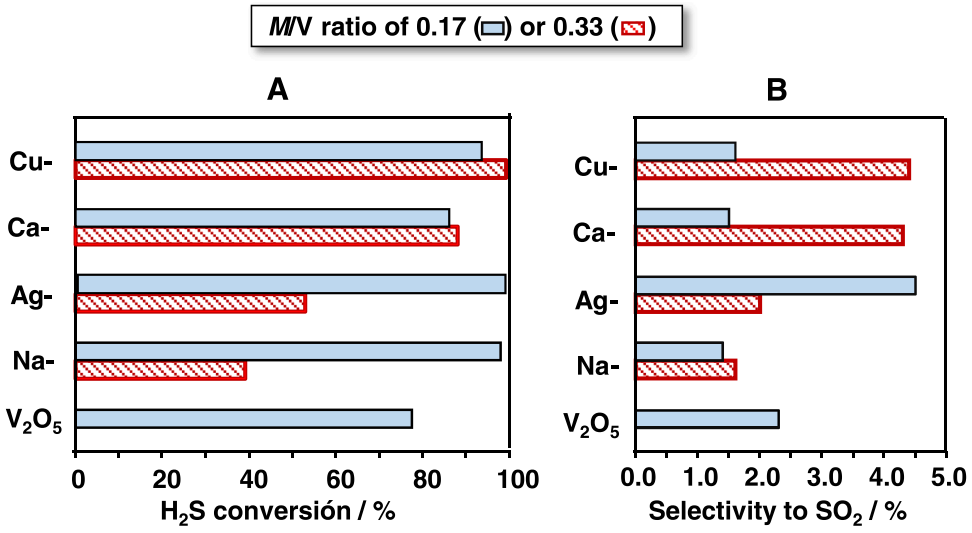

Fig. 8. Variation of the hydrogen sulfide conversion (A) and selectivity to SO_2 (B) at a time on stream of 120 min during the partial oxidation of hydrogen sulfide over vanadium bronze catalysts with a *M*/V ratio of 0.17 or 0.33 (*M*= Ag, Cu, Ca). For comparison the results over an undoped vanadium oxide (**V_2O_5** sample) and Na-doped catalysts, previously studied [20], are also included.

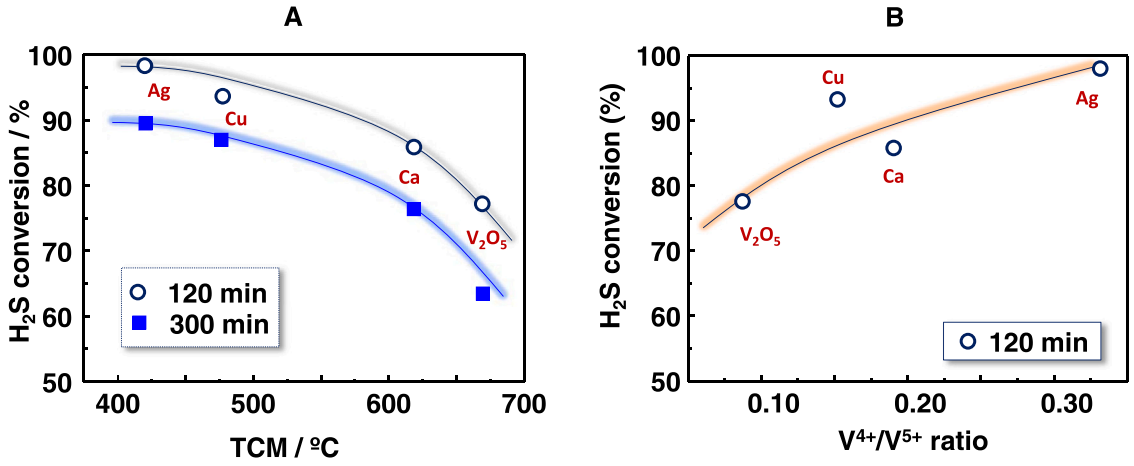

Fig. 9. Variation of the hydrogen sulfide conversion over modified vanadium oxide bronzes with *M*/V ratio of 0.17 (*M*= Ag, Cu, Ca). **A)** Hydrogen sulfide conversion (at a time on stream of 120 or 300 min) vs. the temperature of the first maximum hydrogen consumption in the TPR-H_2 (TCM, °C, in Table 1). **B)** Hydrogen sulfide conversion (at 120 min) vs. the V^{4+}/V^{5+} molar ratio of catalysts, determined by XPS (Table 2). For comparison the results over an undoped vanadium oxide (V_2O_5) are also included.

the β-V_2O_5 structure ($Cu_{0.261}V_2O_5$ phase) leads to more active and selective catalyst for the partial oxidation of H_2S.

Fig. 8A compares the H_2S conversion values at 120 min of reaction time for all the catalysts, including the catalysts doped with Na^+, previously studied [19]. The H_2S conversion of the *M*-doped catalysts is higher than 85 %, except for **Ag/V-0.33** and **Na/V-0.33**, which besides undoped vanadium oxide (i.e. **V_2O_5** sample) display a lower activity. Indeed, the two samples, **Ag/V-0.33** and **Na/V-0.33**, contain other crystalline phases besides the β-bronze structure. Then, the catalytic activity decreases according to (Fig. 8A): **Cu/V-0.33** ≈ **Ag/V-0.17** ≈ **Na/V-0.17** > **Cu/V-0.17** > **Ca/V-0.17** ≈ **Ca/V-0.33** > **V_2O_5** > **Ag/V-0.33** > **Na/V-0.33**.

Additionally, Fig. 8B displays the SO_2 selectivity values for these catalysts. As already mentioned, the SO_2, which is also an undesired pollutant, is the only by-product obtained by the elemental sulfur combustion [4]. As it can be seen, the selectivity to SO_2 is less than 2.0 % for **Cu/V-0.17**, **Ca/V-0.17, Na/V-0.17** or **Na/V-0.33** catalysts, lower than that found for **V_2O_5**. These results suggest that the monoclinic β-$M_xV_2O_5$ vanadium oxide is selective to elemental sulfur, being almost negligible both the direct conversion of H_2S to SO_2 and/or the further sulfur combustion to SO_2. Moreover, for the Cu-containing catalysts, the formation of SO_2 is much less favored in the sample that only contains the β-$M_xV_2O_5$ phase (i.e. **Cu/V-0.17**).

Fig. 9 A shows the H_2S conversion at 120 and 300 min of reaction time of the catalysts with *M*/V= 0.17 against the temperature of the first maximum hydrogen consumption in TPR-H_2 experiments (presented as TCM in Table 1). As a general trend, the H_2S conversion increases along with the catalyst's reducibility. In this sense, the catalytic activity decreases following this trend: **Ag/V-0.17** > **Cu/V-0.17** > **Ca/V-0.17** > **V_2O_5**.

Fig. 9B presents the catalytic activity in the H_2S oxidation as a function of the V^{4+}/V^{5+} ratio at 120 min of reaction time, which shows that the H_2S conversion increases as the V^{4+} concentration in the sample increases, suggesting that this behavior is related to the formation of the β-$M_xV_2O_5$ bronze structure.

3.3. Characterization of used catalysts

To shed some light on the catalysts' deactivation during partial oxidation of H_2S to elemental sulfur, all the catalysts (i.e. ***M*/V-0.17** and ***M*/V-0.33** series and **V_2O_5** sample) have been characterized by XRD and XPS after 5 h of reaction time at 180 °C. In this sense, Fig. 10 shows the XRD pattern of used catalysts.

The β-$M_xV_2O_5$ structure is maintained in all ***M*/V-0.17** catalysts, although a slight decomposition of **Cu/V-0.17** sample into CuS and V_4O_9 is observed (Fig. 10 B). Furthermore, diffraction peaks corresponding to elemental sulfur, probably deposited on the catalysts' surface after the reaction, can also be distinguished.

On the other hand, several crystalline phases can be discriminated in the ***M*/V-0.33** series after the catalytic tests, although the β-$M_xV_2O_5$ phase is still the majority. The **Ag/V-0.33** catalyst presents diffraction peaks corresponding to Ag_2S, as well as a minority of $Ag_{1.2}V_3O_8$, suggesting the partial decomposition of the latter into Ag_2S and β-$Ag_{0.333}V_2O_5$ (Fig. 10 A). Regarding the Cu catalysts, both **Cu/V-0.17** and **Cu/V-0.33** samples show small differences in their XRD patterns despite presenting a similar catalytic activity. However, the characterization of the used samples confirmed that the **Cu/V-0.17** catalyst conserves the β-$Cu_{0.261}V_2O_5$ structure, whereas the CuV_2O_6 phase, present in fresh **Cu/V-0.33** catalyst, is transformed into β-$Cu_{0.261}V_2O_5$ and CuS (Fig. 10 B) [37]. Interestingly, the XRD pattern of the

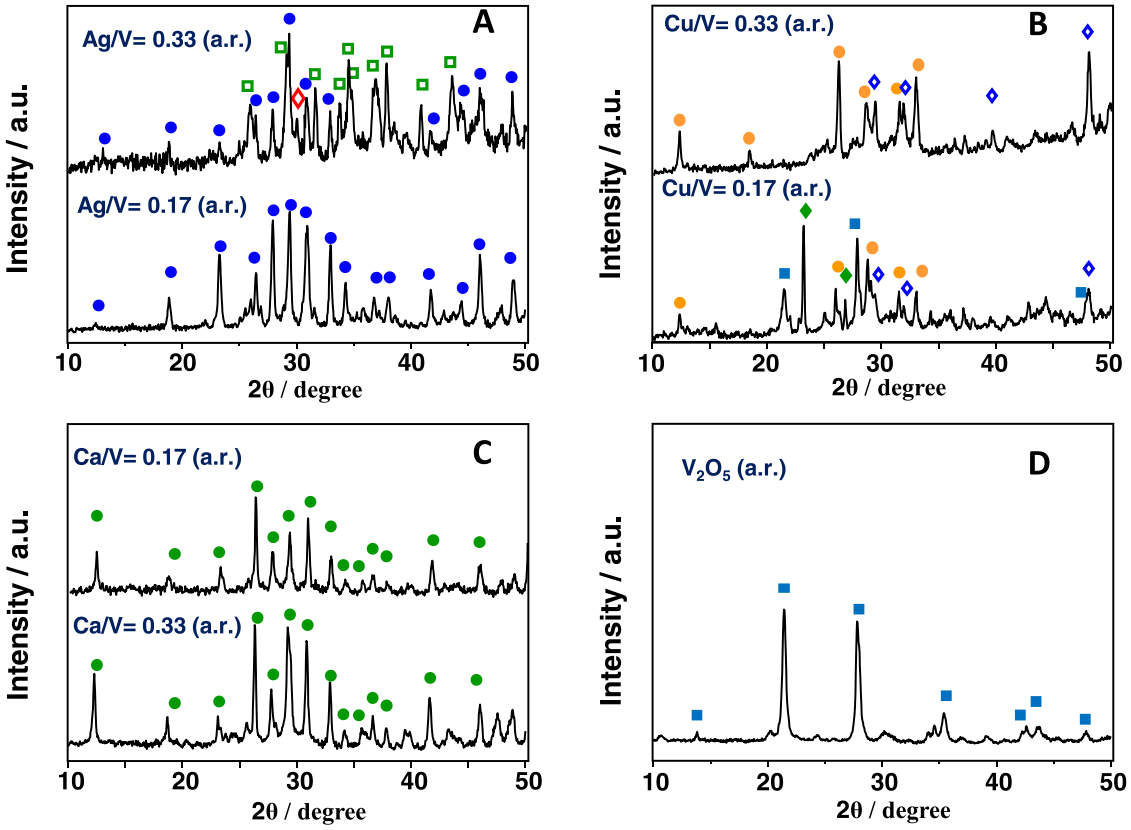

Fig. 10. XRD pattern of used catalysts: a) Ag-doped; b) Cu-doped; c) Ca-doped; and d) V_4O_9 catalysts. Symbols: (■) V_4O_9 (JCPDS: 00–23–0720); (●) β-$Ca_{0.17}V_2O_5$ (JCPDS: 00–26–1165); (●) β-$Cu_{0.261}V_2O_5$ (JCPDS: 1–79–0796); (●) β-$Ag_{0.33}V_2O_5$ (JCPDS: 00–81–1740); (♦) S (JCPDS: 00–08–0247); (◊) CuS (JCPDS: 00–06–0464); (◊) $Ag_{1.2}V_3O_8$ (JCPDS: 00–88–0686), (□) Ag_2S (JCPDS: 00–14–0072).

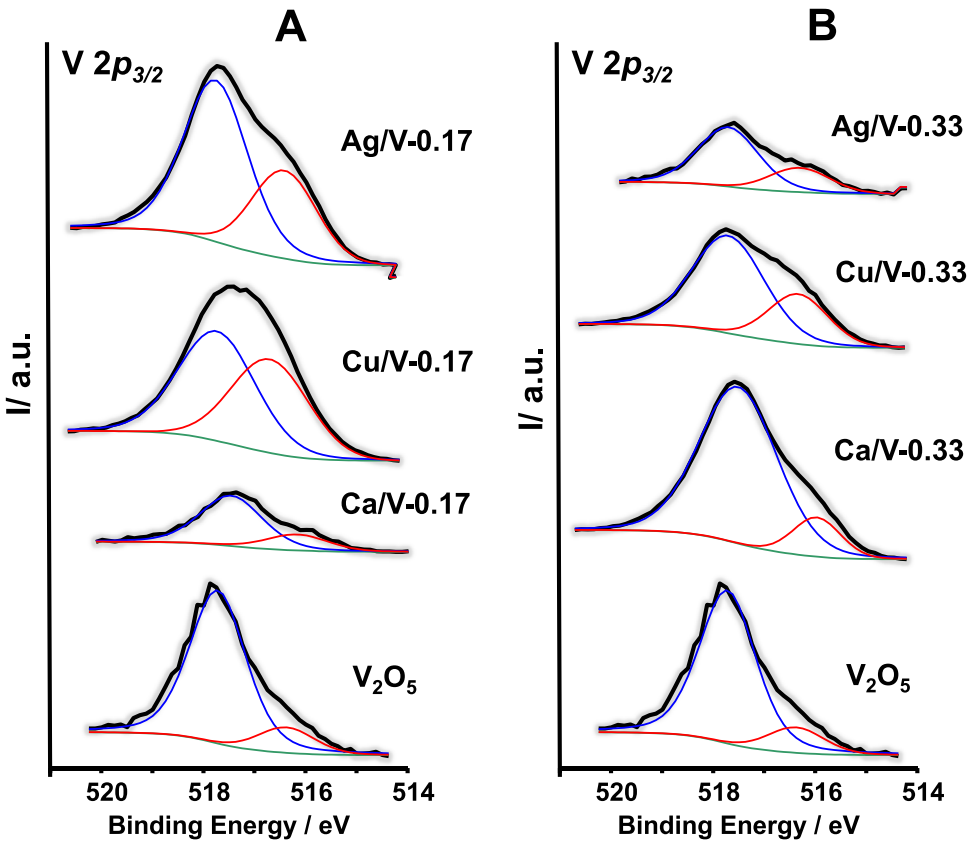

Fig. 11. XPS V $2p_{3/2}$ core level spectra of the used ***M*/V-0.17** (left) and used ***M*/V-0.33** (right) catalysts (*M*= Ag, Cu, or Ca). For comparison it has been also included that achieved from V_2O_5, after reaction. After catalytic tests (Figs. 6 and 7).

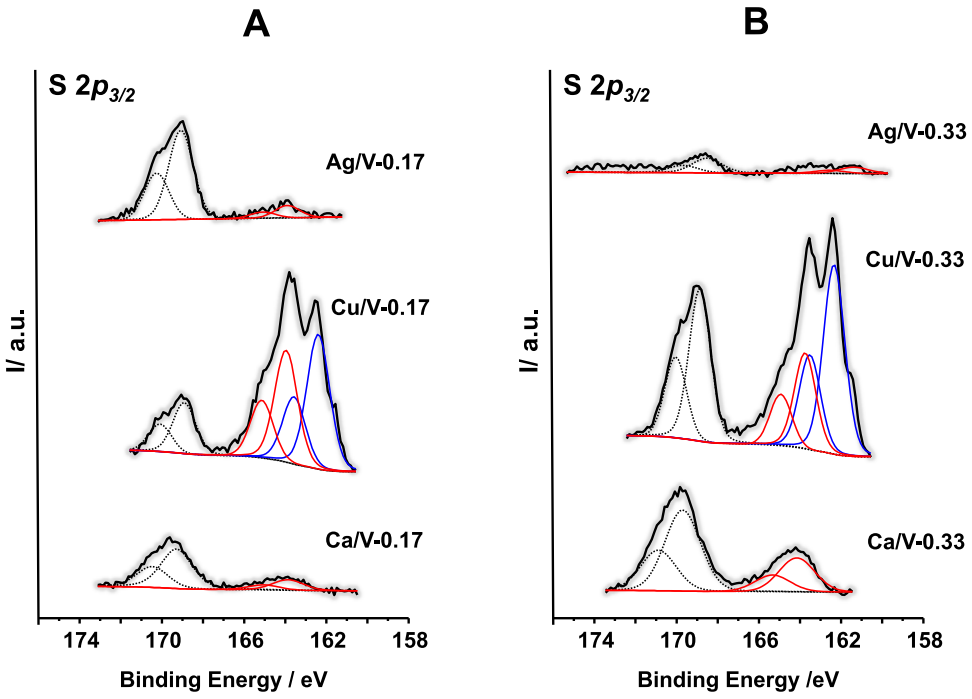

Fig. 12. XPS S 2*p* core level spectra of the used ***M*/V-0.17** (A) and used ***M*/V-0.33** (B) catalysts (*M*= Ag, Cu, or Ca). After catalytic tests in Figs. 6 and 7.

Ca/V-0.33 sample did not show any other crystalline phase than the β-$Ca_{0.17}V_2O_5$ pattern (Fig. 10 C). In addition to this, it can also be seen that the **V_2O_5** sample was completely transformed after reaction into the V_4O_9 crystalline phase (Fig. 10 D), as previously reported [14].

The XPS spectra of the V $2p_{3/2}$ and the S 2*p* core levels of the used catalysts are presented in Figs. 11 and 12, respectively, whereas the results obtained from the deconvolution of both V $2p_{3/2}$ and S 2*p* signals are presented in Table 2. The analysis of the V $2p_{3/2}$ (Fig. 11) bands for

both **M/V-0.17** and **M/V-0.33** series after the catalytic test shows an increase in the relative intensity of the signal at binding energy 516.3 eV, assigned to V^{4+} species [32], confirming a partial reduction of the V^{5+} species under the reaction conditions.

In addition, the XPS analysis of the S 2*p* core level spectra of the ***M*/V-0.17** and ***M*/V-0.33** series after reaction, are presented in Fig. 12A and B, respectively. In that figure, two doublets at 163.3–163.7 eV and 164.4–164.9 eV, and at 168.3–168.6 and 169.5–169.8 eV associated to the presence of elemental sulfur and sulfate species (SO_4^{2-}) [38,39], respectively, are observed in all Ag-, Ca- and Cu-containing catalysts for ***M*/V-0.17** and ***M*/V-0.33** (Fig. 12A and B). However, the spectra of **Cu/V-0.17** and **Cu/V-0.33** catalysts show a third doublet at binding energies of 161.8 and 163.0 eV, which can be assigned to S^{2-} species [8]. Quantitative results and distribution of species are presented in Table 2.

Overall, the presence of elemental sulfur, sulfide and sulfate species suggests that the accessibility of H_2S to the active centers could be diminished during reaction, thus causing the partial deactivation of the catalysts with time.

According to these results, catalysts synthesized from acetate (i.e. Ag and Cu) and oxalate (i.e. Ca) salts with a *M*/V atomic ratio of 0.17 or 0.33 show interesting catalytic properties in the partial oxidation of H_2S to elemental sulfur, presenting H_2S conversions beyond 80 % and remarkable stability during 5 h of reaction time.

In general, the most active **Ag/V-0.17**, **Cu/V-0.17** and **Ca/V-0.33** catalysts present the β-$M_xV_2O_5$ bronze as the majority crystalline phase. Although the V^{4+}/V^{5+} atomic ratio of $Me_xV_2O_5$ bronze is in the range 0.20–0.30 (see Table 2), both Cu-catalysts, **Cu/V-0.17** and **Cu/V-0.33**, show a V^{4+}/V^{5+} ratio lower than 0.20, as a consequence of the presence of multiple vanadates and/or V_2O_5 as impurities.

On the other hand, some crystalline phases different from the β-$M_xV_2O_5$, such as $Ag_{1.2}V_3O_8$ (in **Ag/V-0.33** catalyst), are stable during the partial oxidation of H_2S, whereas V_2O_5 and CuV_2O_6 are transformed into V_4O_9 and β-$Cu_{0.261}V_2O_5$, respectively. Moreover, the catalysts that present both crystalline phases (i.e. V_2O_5 and CuV_2O_6), showed a higher V^{4+}/V^{5+} ratio after the reaction (Table 2), suggesting the partial reduction of the V^{5+} species.

Therefore, the catalysts consisting on the monoclinic bronze phase (β-$Ag_{0.333}V_2O_5$, β-$Ca_{0.17}V_2O_5$ and β-$Cu_{0.261}V_2O_5$) are active, selective and stable under catalytic conditions in the partial oxidation of H_2S. In addition, the catalytic activity increases with the reducibility of the sample (Fig. 9), which seems to be related to the presence of V^{4+}-O-V^{5+} pairs in β-$M_xV_2O_5$, which are the active centers in the oxidation of H_2S to elemental sulfur, thus avoiding consecutive oxidation to SO_2.

However, no clear correlation has been found between the V^{4+}/V^{5+} ratio (in fresh or in used catalysts) and the selectivity to sulfur, suggesting that the presence of the dopant must also have some influence on both the partial reactions of H_2S to sulfur as in the combustion of elemental sulfur to SO_2.

4. Conclusions

In conclusion, it has been shown that the metal-promoted vanadium oxide bronzes, especially those with the crystalline phases $Ag_{0.333}V_2O_5$ and $Cu_{0.261}V_2O_5$, are active, selective and stable catalysts for the partial oxidation of H_2S to elemental sulfur. These catalysts show better catalytic performance, where the selectivity to sulfur can be beyond 95%, than those traditionally used for this process (i.e. V_2O_5).

The presence of V^{4+}-O-V^{5+} pairs in these oxides has a significant effect on the catalytic properties by preventing the overoxidation of elemental sulfur to SO_2. Moreover, these results suggest that the presence of Ag or Cu cations could favor not only the redox process (thus increasing the catalytic activity) but also the stability of these pairs (the metal cations stabilize the V^{4+} species).

The catalytic behavior of the catalysts promoted with Ca, with Ca/V ratios of 0.17 and 0.33, with the crystalline bronze $Ca_{0.17}V_2O_5$ structure, can be explained by an enrichment in the Ca^{2+} cations of the catalysts' surface, and that seems to favor the S^{2-} and/or S^0 desorption. However, high amounts of sulfate anions (SO_4^{2-}) are also found, probably stabilized by the Ca^{2+} cations on the catalysts' surface, may facilitate the lower sulfur selectivity and thus, the greater formation of SO_2.

CRediT authorship contribution statement

L. Ruiz-Rodríguez: Investigation, Formal analysis, writing – review, editing. **A. de Arriba:** Investigation, Formal analysis, Writing – review & editing. **A. Vidal-Moya:** Methodology, Investigation, Formal analysis, writing. **T. Blasco:** Methodology, Investigation, Formal analysis, writing. **E. Rodríguez-Castellón:** Conceptualization, Supervision, writing – review & editing. **J.M. Lopez Nieto:** Conceptualization, Supervision, Project Administration, writing – review & editing.

Declaration of Competing Interest

The authors declare that they have no known competing financial interests or personal relationships that could have appeared to influence the work reported in this paper.

Data availability

Data will be made available on request.

Acknowledgements

The authors would like to acknowledge the Ministerio de Ciencia e Innovación of Spain (TED2021-130756B-C31, TED2021-130756B-C32 and MAT2017-84118-C2-1-R projects). Authors from ITQ also thank Project SEV-2016–0683 for supporting this research. A.A. acknowledges Severo Ochoa Excellence Program for his fellowship (BES-2017-080329) and Dr. Ferran Sabaté from ITQ for his assistance with the EPR data treatment.

Appendix A. Supporting information

Supplementary data associated with this article can be found in the online version at doi:10.1016/j.apcata.2022.118900.

References

[1] X. Zhang, Y. Tang, S. Qu, J. Da, Z. Hao, H_2S-selective catalytic oxidation: catalysts and processes, ACS Catal. 5 (2015) 1053–1067.
[2] J.H. Yang, Hydrogen sulfide removal technology: a focused review on adsorption and catalytic oxidation, Korean J. Chem. Eng. 38 (2021) 674–691.
[3] A. Piéplu, O. Saur, J.C. Lavalley, O. Legendre, C. Nédez, Claus catalysis and H_2S selective oxidation, Catal. Rev. - Sci. Eng. 40 (1998) 409–450.
[4] J. Wieckowska, Catalytic and adsorptive desulphurization of gases, Catal. Today 24 (1995) 405–465.
[5] A.A. Davydov, V.I. Marshneva, M.L. Shepotko, Metal oxides in hydrogen sulfide oxidation by oxygen and sulfur dioxide I. The comparison study of the catalytic activity. Mechanism of the interactions between H_2S and SO_2 on some oxides, Appl. Catal. A-Gen. 244 (2003) 93–100.
[6] K.V. Bineesh, S.-Y. Kim, B.R. Jermy, D. Won Park, Catalytic performance of vanadia-doped titania-pillared clay for the selective catalytic oxidation of H_2S, J. Ind. Eng. Chem. 15 (2009) 207–211.
[7] K.V. Bineesh, M. Kim, G.-H. Lee, M. Selvaraj, K. Hyun, D.-W. Park, Production of elemental sulfur and ammonium thiosulfate by the oxidation of H2S containing water vapor and ammonia over V/Zr-PILC catalysts, J. Ind. Eng. Chem. 18 (2012) 1845–1850.
[8] M.D. Soriano, J. Jiménez-Jiménez, P. Concepcion, A. Jiménez-López, E. Rodríguez-Castellón, J.M. López, Nieto, Selective oxidation of H2S to sulfur over vanadia supported on mesoporous zirconium phosphate heterostructure, Appl. Catal. B-Environ. 92 (2009) 271–279.
[9] Z. Fan, H. Guo, K. Fang, Y. Sun, Efficient V_2O_5/TiO_2 composite catalysts for dimethoxymethane synthesis from methanol selective oxidation, RSC Adv. 5 (2015) 24795–24802.
[10] T. Kane, J. Guerrero-Caballero, A. Löfberg, H2S chemical looping selective and preferential oxidation to sulfur by bulk V_2O_5, Appl. Catal. B-Environ. 265 (2020), 118566.
[11] V. Palma, D. Barba, Low temperature catalytic oxidation of H_2S over V_2O_5/CeO_2 catalysts, Int. J. Hydrog. Energy 39 (2014) 21524–21530.

[12] S. Phatyenchuen, B. Pongthawornsakun, J. Panpranot, P. Praserthdam, Effect of transition metal dopants (M= Nb, La, Zr, and Y) on the M-TiO_2 supported V_2O_5 catalysts in the selective oxidation of H_2S to elemental sulfur, J. Environ. Chem. Eng. 6 (2018) 5655–5661.
[13] B. Pongthawornsakun, S. Phatyenchuen, J. Panpranot, P. Praserthdam, The low temperature selective oxidation of H2S to elemental sulfur on TiO_2 supported V_2O_5 catalysts, J. Environ. Chem. Eng. 6 (2018), 1414-1413.
[14] J.P. Holgado, M.D. Soriano, J. Jiménez-Jiménez, P. Concepción, A. Jiménez-López, A. Caballero, E. Rodríguez-Castellón, J.M. López, Nieto, Operando XAS and Raman study on the structure of a supported vanadium oxide catalyst during the oxidation of H_2S to Sulphur, Catal. Today 155 (2010) 296.
[15] H. Eom, S.M. Lee, H. Kang, Y.H. Lee, S.W. Chang, S.S. Kim, Effect of VOx surface density and structure on VOx/TiO_2 catalysts for H_2S, Sel. Oxid. React. J. Ind. Eng. Chem. 92 (2020) 252–262.
[16] M.D. Soriano, J.A. Cecilia, A. Natoli, J. Jiménez-Jiménez, J.M. López Nieto, E. Rodríguez-Castellón, Vanadium oxide supported on porous clay heterostructure for the partial oxidation of hydrogen sulphide to sulfur, Catal. Today 254 (2015) 36–42.
[17] X. Zhan, Y. Tang, N. Qiao, Y. Li, S. Qu, Z. Hao, Comprehensive study of H_2S selective catalytic oxidation on combined oxides derived from Mg/Al-$V_{10}O_{28}$ layered double hydroxides, Appl. Catal. B 176–177 (2015) 130–138.
[18] J.H. Yang, H.J. Lee, H.S. Lee, S.-C. Jeon, Y.-S. Han, Precise control of heat-treatment conditions to improve the catalytic performance of V_2O_5/TiO_2 for H_2S removal, J. Hazard. Mater. 416 (2021), 125974.
[19] M.D. Soriano, J.M. López Nieto, F. Ivars, P. Concepción, E. Rodriguez-Castellón, Alkali-promoted V_2O_5 catalysts for the partial oxidation of H_2S to Sulphur, Catal. Today 192 (2012) 28–35.
[20] M.D. Soriano, E. Rodríguez-Castellón, E. García-González, J.M. López Nieto, Catalytic behavior of NaV_6O_{15} bronze for partial oxidation of hydrogen sulfide, Catal. Today 238 (2014) 62–68.
[21] M.D. Soriano, A. Vidal-Moya, E. Rodríguez-Castellón, F.V. Melo, M.T. Blasco, J. M. López Nieto, Partial oxidation of hydrogen sulfide to sulfur over vanadium oxides bronzes, Catal. Today 259 (2015) 237–244.
[22] P.M. Marley, G.A. Horrocks, K.E. Pelcher, S. Banerjee, Transformers: the changing phases of low-dimensional vanadium oxide bronzes, Chem. Commun 51 (2015) 5181–5198.
[23] U. Bentrup, A. Martin, G.U. Wolf, Comparative study of the thermal and redox behaviour of alkali-promoted V_2O5 catalysts, Thermoch. Acta 398 (2003) 131–143.
[24] T. Ono, Y. Tanaka, T. Takeuchi, K. Yamamoto, Characterization of K-mixed V2O5 catalyst and oxidative dehydrogenation of propane on it, J. Mol. Catal. A Chem. 159 (2000) 293–300.
[25] M. Nohair, D. Aymes, P. Perriat, B. Gillot, Infrared spectra-structure correlation study of vanadium-iron spinels and their oxidation products, Vib. Spectrosc. 9 (1995) 181–190.
[26] M.K. Chine, F. Sedini, N. Gharbi, Solvothermal synthesis of V4O9 flake-like morphology and its photocatalytic application in the degradation of methylene blue, Mat. Res. Bull. 47 (2012) 3422–3426.
[27] J.C. Badot, D.G.F. Bourdeau, N. Baffier, A. Tabuteau, Electronic properties of $Na_{0.33}V_2O_5$ bronze obtained by sol-gel process, J. Solid State Chem. 92 (1991) 8–17.
[28] D.A. Solis-Casados, L. Escobar-Alarcón, A. Infantes-Molina, T. Klimova, L. Serrato-Garcia, E. Rodríguez-Castellón, S. Hernández-López, A. Dorazco-González, Synthesis and characterization of Ag-modified V_2O_5 photocatalytic, Mater. J. Chem. 2017 (2017) 5849103.
[29] Ch.J. Patridge, Ch. Jaye, H Zhang, A.C. Marschilok, D.A. Fischer, E.S. Takeuchi, S. Banerjee, Synthesis, structural characterization, and electronic structure of single-crystalline $Cu_xV_2O_5$ nanowires, Inorg. Chem. 48 (2009) 3145–3152.
[30] F. Coustier, J. Hill, B.B. Owens, S. Passerini, W.H. Smyrl, Doped vanadium oxides as host materials for lithium intercalation, J. Electrochem. Soc. 145 (1999) 1355.
[31] M. Galván-Ruiz, J. Hernández, L. Baños, J. Noriega-Montes, E. Rodríguez-García, Characterization of calcium carbonate, calcium oxide, and calcium hydroxide as starting point to the improvement of lime for their use in construction, J. Mater. Civ. Eng. 21 (2009) 694–698.
[32] G. Silversmit, D. Depla, H. Poelman, G.B. Marin, R. De Gryse, Determination of the V2p XPS binding energies for different vanadium oxidation states (V^{5+} to V^{0+}), J. Electron Spectrosc. 135 (2004) 167–175.
[33] E.A. Souza, R. Landers, M.H. Tabacniks, L.P. Cardoso, A. Gorenstein, Cathodic behavior of co-sputtered Cu/V oxides thin films, Electrochim. Acta 51 (2006) 5885–5891.
[34] A. Adamski, P. Zapala, L. Chmielarz, J.A.J. Rodríguez, G. Djéga-Mariadassou, Z. Sojka, The effect of zirconia and niobia supports on the catalytic activity of surface VOx species in total oxidation of model volatile organic compounds, Catal. Today 176 (2011) 318–323.
[36] V.I. Merupo, S. Velumani, K. Ordon, N. Errien, J. Szade, A.H. Kassiba, Structural and optical characterization of ball-milled copper-doped bismuth vanadium oxide ($BiVO_4$), CrystEngComm 17 (2015) 3366–3375.
[37] Z. Li, Li Mi, W. Chen, H. Hou, C. Liu, H. Wang, Z. Zheng, C. Shen, Three-dimensional CuS hierarchical architectures as recyclable catalysts for dye decolorization, CrystEngComm 14 (2012) 3965–3971.
[38] M. Fantauzzi, B. Elsener, D. Atzei, A. Rigoldi, A. Rossi, Exploiting XPS for the identification of sulfides and polysulfide, RSC Adv. 5 (2015) 75953–75963.
[39] J.F. Moulder, W.F. Stickle, P.E. Sobol, K.D. Bomben, Standard Spectra for Identification and Interpretation of XPS Data, Perkin Elmer, Eden Prairie, MN (1992).

Further reading

[1] A. Bruckner, In situ electron paramagnetic resonance: a unique tool for analyzing structure–reactivity relationships in heterogeneous catalysis, Chem. Soc. Rev. 39 (2010) 4673–4684.